Interaction of a Supersonic Stream and a Transverse Supersonic Jet

A. F. CHARWAT*
University of California at Los Angeles, Los Angeles, Calif.
AND
J. ALLEGRE†
Centre National de la Recherche Scientifique, Paris, France

The present experimental study of a transverse jet discharging into a supersonic nozzle was undertaken to clarify the details of the flow. Results of wall and impact pressure measurements throughout the core of the interaction field, as well as flow visualization tests, are reported for 11 tests differing as systematically as possible by the injected mass rate, injection station Mach number, and primary to secondary stagnation pressure ratio. These measurements are used in an effort to reconstruct the true structure of the flow and suggest the following characteristic features of it. The penetration and turning of the secondary (supersonic) jet is governed by the dynamics of the shock structure occurring in the free-expansion plume and it is not a simple function of jet momentum. The mixing region downstream of injection contains a "horseshoe" vortex separating the inner (jet) flow from the outer (freestream) flow near the nozzle wall. The entire interaction region is enveloped by a nearly ogival shock, the gross properties of which, to the first approximation, depend (nonlinearly) on the injected momentum, the freestream pressure, and the freestream velocity at the injection station.

Nomenclature

A = cross-sectional area of nozzle; A^*: local sonic area
E = energy per unit length (blast wave analogy)
h = specific enthalpy
K = empirical constant [defined by Eq. (6)]
M = Mach number
m = mass flow rate
P = pressure, P_0: stagnation pressure; P_t: impact (total-tube) pressure
R_s = radius of the leading shock (origin at the wall at $\theta = 0$)
R_{so} = reference radius [defined by Eq. (5)]
T = temperature, T_0: stagnation temperature
x = axial (streamwise) coordinate, origin on the centerline of the secondary injection port
x^* = axial (streamwise) coordinate of the origin of the leading shock for the blast-wave analogy
X = axial (streamwise) distance from the origin of the leading shock for the blast-wave analogy: $X = x - x^*$
y = coordinate normal to the nozzle wall
θ = polar coordinate, measured from the nozzle axis

Subscripts

j = denotes quantities pertaining to the secondary jet
i = denotes quantities pertaining to the undisturbed (no injection) flow in the expansion nozzle
∞ = "equivalent" uniform flow quantities used in the blast-wave analogy

Quantities pertaining to the undisturbed flow in the primary expansion nozzle are without a subscript.

Received January 21, 1964; revision received July 29, 1964. The experiments reported herein were conducted in the Laboratoire d'Aerothermique du Centre National de Recherches Scientifiques, Paris, France, during the senior author's appointment as Visiting Professor to the University of Paris. He gratefully acknowledges the support of the John Simon Guggenheim Memorial Foundation. The authors thank E. Brun, Director of the laboratory, for making the facility available and for his encouragement and support.

* Professor. Associate Fellow Member AIAA.
† Research Assistant, Laboratoire d'Aerothermique.

Introduction

THE present is an investigation of the flow field set up by a transverse gas jet issuing into a supersonic stream. Such flows occur in applications to jet-flaps and to thrust vector control for rocket motors. In that case, the secondary jet issues into the divergent part of the thrust nozzle; the interaction produces an asymmetric force field that results in a side-thrust greater than that produced by the secondary jet alone.

A number of experiments on secondary jet injection have been published,[1–6] and several analytical models of the phenomenon have been proposed.[7–9] However, both provide little information on the detailed structure of the interaction field. Such information is needed; for example, it is known that significantly different wall-pressure patterns and side forces are obtained with liquid and gaseous secondary jets. The difference is ascribable to evaporation phenomena, which depend on local thermodynamic conditions throughout the core of the flow.

Accordingly, the present experiments were undertaken to clarify some aspects of this internal structure of the flow. The flow field was traversed in several sectional planes normal to the primary flow and in the meridional plane parallel to the primary flow containing the secondary jet axis. Wall pressure distributions and flow-visualization tests were conducted. The experiments included 11 tests differing as systematically as possible by the value of three principal parameters: the injected mass flow rate, the injection station Mach number, and the primary-to-secondary flow stagnation pressure ratio.

The study leads to a description of the initial interaction zone immediately over the injection port. It indicates the existence of a spiral mixing zone and provides preliminary estimates of the penetration height of the disturbance into the main flow. It also yields some quantitative correlations with Broadwell's[8] blast-wave analogy model of the interaction.

Table 1 Summary of test settings[a]

Test Denomination		A	B	C	D	E
Secondary nozzle throat A_j^*, mm		5.0	3.0	5.0	3.0	5.0
Secondary Mach no. at nozzle exit M_j		1.0	1.0	1.0	2.06	1.0
Primary Mach. no. at injection station M_i		2.12	2.12	2.41	2.12	2.61
Secondary/primary stagnation pressure ratio P_{j0}/P_0	−1	1.0	1.0	1.0	1.0	1.0
	−2	0.725	0.725	0.725	...	...
	−3	0.36	0.36	0.36	...	...

[a] For all tests, P_0 = 1 atm and T_0 = 520°R.

Experimental Equipment and Technique

The experiment was conducted using a 5° half-angle, conical primary nozzle. Because it was not the intention to optimize the lateral-force coefficients or reproduce a practical thrust-nozzle configuration, a small divergence angle was chosen in order to minimize the axial pressure gradients. This minimized the effects of these gradients on the intermixing of the streams.

The stagnation conditions for the primary flow were atmospheric in all tests. The nozzle discharged into a vacuum system at a pressure sufficient to maintain a small degree of underexpansion at the nozzle exit. The primary nozzle had a 3-cm-diam circular throat. The undisturbed pressure distribution in the nozzle confirmed area-ratio calculations closely. The boundary layer was presumed to be fully turbulent.

Table 1 shows the differences in configuration and stagnation conditions for the five groups of tests. The secondary nozzles used in tests A, B, C, and E were sharp-edged sonic orifices with a profiled inlet from a secondary stagnation chamber in which the pressure could be varied. The 3-mm throat orifices (test B) were obtained by slipping an insert into the basic 5-mm throat orifice (tests A, C, and E). A convergent-divergent supersonic nozzle with a 3-mm throat and an 8° half-angle expansion cone was used in test D. Three locations of the secondary injection port were used; tests A, C, and E are identical except for this factor.

Measurements consisted of wall static pressure and total-tube pressure traverses. Wall pressures were obtained at each 30° interval around the circumference and at intervals of 7.5 mm (near the injection port) and 15 mm (in the far-downstream region) axially. Impact pressure measurements were made at intervals of approximately 0.5 mm with the precision in the probe location of the same order of magnitude. The probe was mounted on a traversing mechanism located in the discharge chamber downstream of the nozzle exit so as to avoid interferences with the nozzle wall boundary layer. The diameter of the probe stem was gradually reduced to a stainless-steel hypodermic needle, 2 cm long, with a 1-mm flattened opening. At least two complete loops were made for each traverse to avoid errors due to backlash in the traversing leadscrew. All tests at a given axial station were performed starting from a fixed (arbitrary) origin in the flow in order to increase the precision in the relative positioning of the mechanism. This arbitrary origin was related to the wall at the end of the series of tests performed at that axial position. All curves are drawn through all of the measured points, although the points themselves are not shown for clarity.

The secondary mass flow rate was calibrated in a special test using a venturi in series with the secondary injection orifice. These measurements showed that, for all tests, the measured flow rate equaled (within 3% accuracy) that calculated for sonic flow through the throat of the secondary orifice.

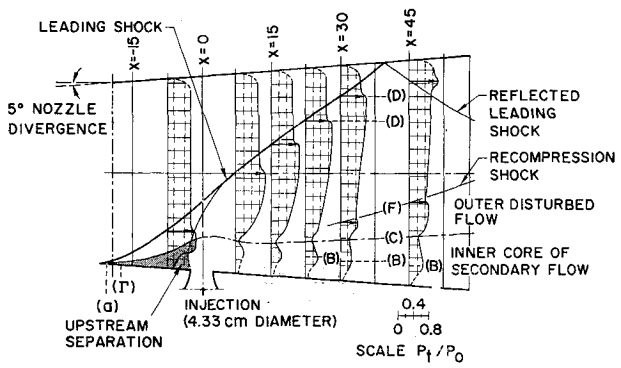

Fig. 1 Impact pressure traverses in the meridional plane (test conditions A1).

Over-All Survey of a Typical Flow

A presentation of the measurements is made below according to a sequence of the three nearly Cartesian coordinates: first, the meridional plane containing the axis of the primary flow and that of the secondary jet; second, sectional planes normal to the axis of the principal flow; and third, the plane

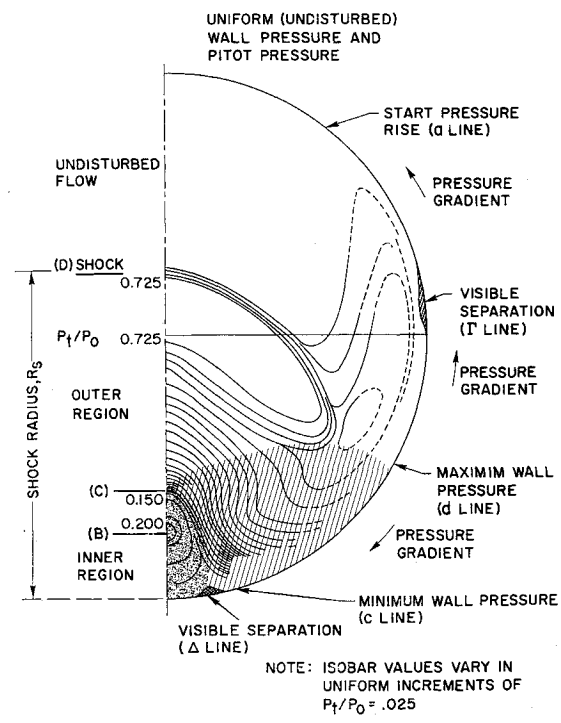

Fig. 2 Distribution of impact pressure over the cross-sectional plane 15-mm downstream of injection (test A1).

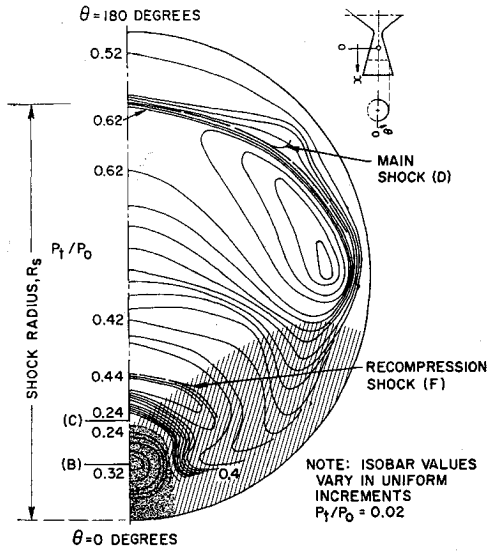

Fig. 3 Distribution of impact pressure over the cross-sectional plane 30-mm downstream of injection (test A1).

of the primary nozzle wall. The configuration of this test is that of test A1 in Table 1.

Figure 1 illustrates a sequence of total-tube pressure traverses in the meridional plane before, at, and after the injection station, as well as after the station at which the leading shock reflects off the opposite side of the primary nozzle. The portion of the flow downstream of the intersection of the leading shock and the $\theta = 90°$ line, is not interesting from the standpoint of practical thrust vector control (TVC) applications; here the force opposes the jet reaction and decreases the desired side thrust.

Figures 2 and 3 are maps of lines of constant impact pressure in sectional planes 15-mm and 30-mm downstream of the injection port. These isobars were drawn from measurements along radii at polar angles 0° (meridional plane), 15°, 30°, 60°, 90°, 135°, and 180°. Annotations on Fig. 2 relate this map to characteristics of the variation of the pressure measured on the wall as well as the meridional plane traverses (Fig. 1).

Impact pressures do not suffice to calculate the local flow velocities, because, in addition to entropy variations, the local direction of the flow is not known. However, the maps of Figs. 2 and 3 portray qualitatively the essential character of the flow field. This may be discussed more effectively, after additional data is reviewed, as follows.

Figure 4 illustrates oil-film flow streaklines along the wall of the primary nozzle. Observation discloses the existence of two separated regions along curves denoted as the Γ and the Δ lines. The oil, once introduced where indicated, will flow as indicated and become permanently trapped along these lines. It is impossible to cause the oil to penetrate the Γ line when injected upstream of it. Between the Γ line and the Δ line, the wall shear (flow velocity in the neighborhood of the wall) is fairly large, and the oil-film is swept to the Δ line reasonably rapidly. A zone of higher and one of lower shear can be distinguished as indicated.

Figure 5 portrays the variation of the static pressure on the wall of the nozzle. The data are presented in the form of ratios of the wall pressure to the local "ideal" wall pressure. In this form, the effect of the pressure gradient along the expansion nozzle is eliminated, and a truer picture of the pressure "disturbance" is obtained. The similarity between Figs. 4 and 5 seems to support this choice of representation.

Comparing Figs. 4 and 5, it is found that the upstream separation (the Γ line) follows the isobar 1.2 very closely. The downstream separation (the Δ line) coincides with the line of minimum wall pressures (the c line). Note that the

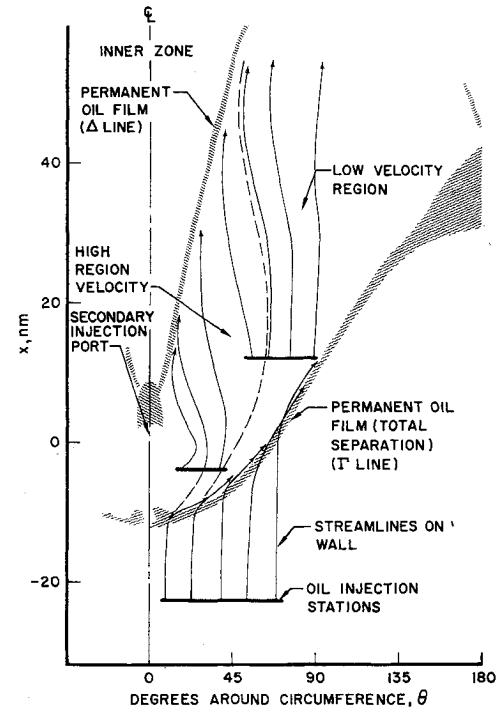

Fig. 4 Study of oil-film streaklines on the surface of the nozzle (test A1).

Γ line is not followed by a decrease in pressure such as one would expect in the case of an ordinary shock-induced boundary-layer separation.

One can now interpret the pressure measurements in terms of the physical character of the flow field. This is done schematically on Fig. 6.

Immediately downstream of the injection orifice, one has an "inner" core of secondary fluid, which is shaded darkly on Fig. 2 and indicated on Fig. 1. This core is well established soon downstream of the orifice and grows relatively

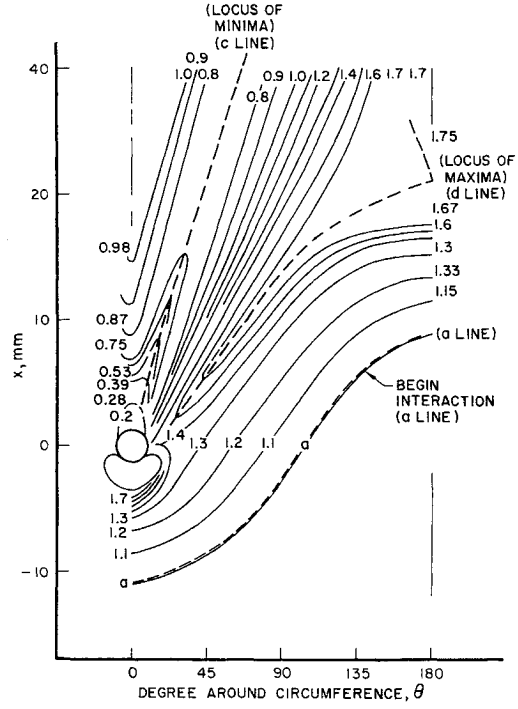

Fig. 5 Lines of constant ratio of wall pressure with injection to wall pressure without injection over the nozzle (test conditions A1).

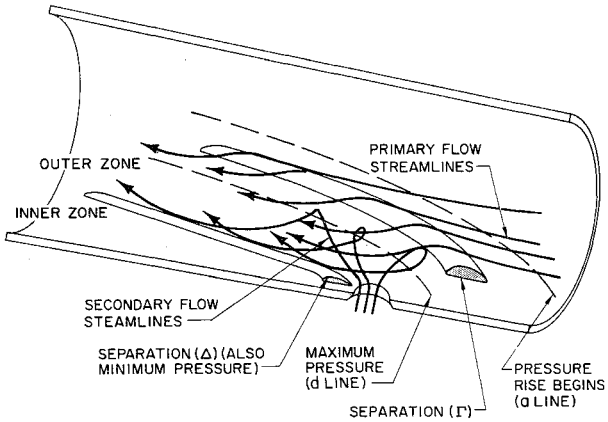

Fig. 6 Schematic representation of the spiral mixing flow.

little with the flow. This core is analogous to an "equivalent body" in models of the flow based on such a concept.

Alongside the inner core, one distinguishes a region in which the isobars of Fig. 2 exhibit an inflection point, shaded lightly on that figure. This suggests a vortex. The jet expands freely sideways at the exit of the injection nozzle, inducing a spiral flow as shown on Fig. 6. This flow returns toward the wall at the location of the wall-pressure peak. The inner boundary of vortical mixing zone with the inner core coincides with the wall-pressure minimum (the c line) and the boundary layer separates locally there (the Δ line) because of the outward radial flow in the vortex.

The inner core and the spiral zone are enveloped by the outer disturbed flow behind the leading shock. Along the wall, the disturbance propagates ahead of the root of the shock in the boundary layer. The boundary layer separates (Γ line), but the free shear layer is then forced back to the wall by the inward radial component of flow at the boundary of the mixing vortex.

Comparative Study of Several Cases

The second part of the program consisted of a comparative study of the 11 settings summarized in Table 1. The flow configurations were chosen in a way that demonstrates the relative role of some principal flow parameters. For instance, tests A3 and B1 involve the same secondary mass flow at different stagnation pressure ratios and nozzle areas. Tests A1, C1, and E1 are identical except for the Mach number at the injection station. Tests B1 and D1 differ only by the secondary nozzle exit plane Mach number, and so on.

The character of the pressure disturbances remained similar for all test settings except in the region immediately over the

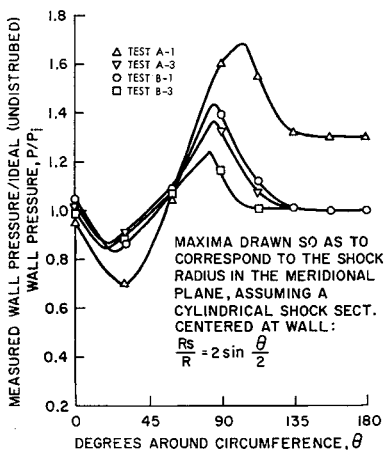

Fig. 7 Behavior of the wall pressure distribution around the circumference 30 mm downstream of injection for various test settings (see Table 1).

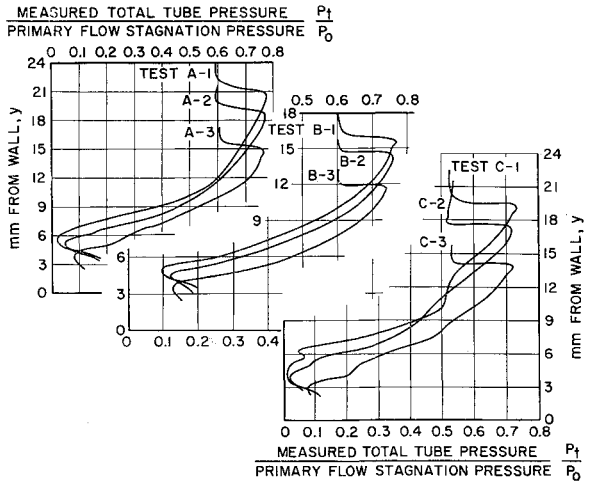

Fig. 8 Behavior of the impact pressure profiles in the meridional plane 9 mm downstream of injection for various test conditions (see Table 1).

secondary orifice, which is discussed separately later. However, no unique, general quantitative similarity parameter could be found. The following was observed:

1) The strength and location of the leading shock in the meridional plane is function of the injected mass flow (momentum) and the injection station Mach number only.

2) The wall pressure distribution is function of the preceding and also (although less strongly) of the ratio of secondary to primary stagnation pressure.

It is surprising to find that, although the pressure jump across the leading shock does not depend explicitly on the stagnation pressure of the secondary jet, the wall pressure maximum does. Figure 7 shows typical circumferential wall pressure surveys, where tests A3 and B1 differ only by the stagnation pressure ratio, whereas A1 and B1 or A3 and B3 differ only by the injectant flow rate. These results confirm the hypothesis of the blast-wave analogy model[8] in the sense that the injected momentum is the principal physical similarity parameter of the over-all problem. The finer structure of the flow within the mixing zone depends, however, on additional parameters. The effect of the stagnation-pressure ratio on the wall pressure can be explained by the flow-

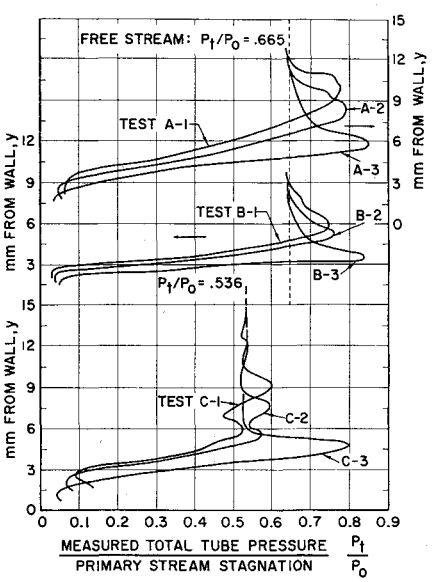

Fig. 9 Behavior of the impact pressure profiles along the centerline of the secondary injection orifice for various test conditions (see Table 1).

Table 2 Shock radius and comparison with blast-wave analogy

Test	R_6 (in mm) at $\theta = 0$ for traverse at 30 mm	9 mm	δ, mm	R_{so}, mm	Calculations x^*, mm	$K_{(30)}$	$K_{(9)}$
A1	37.8	21.3	12	6.21	0.79	4.04	4.2
A2	35.4	19.4	10	5.28	0.09	4.12	4.15
A3	30.0	15.5	6.3	3.73	−1.32	4.13	3.96
B1	30.5	16.1	7.2	3.73	−0.86	4.2	4.22
B2	29.0	14.9	6.0	3.17	−1.41	4.34	4.13
B3	24.5	12.1	3.8	2.24	−2.2	4.35	3.96
C1	32.9	19.4	...	7.72	1.55	3.36	3.63
C2	29.7	17.9	...	6.55	2.95	3.30	3.62
C3	25.9	13.8	8.5	4.64	−0.73	3.41	3.34
E1	31.5	19.2	...	8.9	−0.91	3.18	3.5

structure suggested in Fig. 6. An increase in secondary stagnation pressure (at constant total injected momentum) increases the under-expansion at the nozzle exit, the sideways turning of the secondary flow, and the strength of the vortex. This increases the wall recovery pressure at the stagnation lines of the vortex boundaries.

Figure 8 shows typical traverses of impact pressure in the meridional plane downstream of injection for several settings. A more complete display of this data is given in Ref. 11. The principal characteristics of the profiles, such as the pressure jump across the shock and its location, are given subsequently in tabular form.

The meridional traverses for tests B1 and D1 were identical in all respects at all stations. It is thus possible to add to our general conclusions the following:

3) The degree of expansion in the secondary nozzle bears little influence on the production of the main shock.‡

Flow at the Injection Port

Before attempting to interpret the flow field over the injection orifice, it should be emphasized that the pressure measured by a total-head tube parallel to the nozzle axis changes from impact to approximately static pressure as soon as the instrument penetrates the jet proper (where the flow is parallel to the plane of the pressure tap).

Figure 9 shows the profiles along the jet centerline. Very near the jet exit plane, the pressure (approximately static pressure, see the preceding) decreases with y, indicating that the jet undergoes a free supersonic expansion. The pressure reaches a sharp minimum which must correspond to the location of a shock structure terminating the jet proper. The height can be identified with the point at which, in analogy with supersonic underexpanded jets discharging into still air,[9] the Mach number is such that the stagnation pressure behind a normal shock equals the ambient pressure. An approximate estimate of this height is obtained using known formulas[12] for the evolution of the jet Mach number§ along the centerline and assuming that the recovery pressure is the nozzle static pressure at the injection station. Values of the standoff distance δ so calculated are listed in Table 2 for some cases. They compare well with the heights at which the minimum in the pressure profile is observed and follow the trends of the data as a function of test setting.

The foregoing indicates that the total jet "penetration height" is not a simple function of its momentum. For example, it increases with injection-station Mach number, all other factors remaining constant.

‡ Unfortunately, wall pressures were not recorded for test D1. According to the model discussed previously, changing a "free" expansion to an internal expansion in a convergent-divergent nozzle should have affected the strength of the mixing spiral and resulted in a lower wall pressure maximum.

§ These semiempirical formulas apply to an axisymmetric expansion at the nozzle edge, which is not the case here.

Immediately above the terminal structure in the jet, one expects a layer in which most of the turning of the secondary flow takes place. Figure 9 shows that in this region the measured profiles fall into two distinct groups. Tests A, B, and C3 show a unique maximum reading above which the pressure tends to the freestream impact pressure. Tests C1 and C2 show two peaks instead. The traverses were repeated several times to insure that this difference in their character is real.

Clearly, the upper peak corresponds to the location of the leading shock envelope in the freestream. The occurrence of the middle peak in one group and not in the other reflects a difference in the structure of the interaction region. The present measurements do not provide sufficient information to completely reconstruct this complex interaction field, but it is possible to formulate a theoretical argument that suggests the nature of the difference.

Consider the jet streamtube crossing the nozzle exit plane near the upstream edge in the meridional plane. The pressure in it must equal the local ambient pressure in the upstream separation behind the leading shock in the freestream, P_{su} (see Fig. 10). There are then two possibilities (when the flow across the nozzle exit plane is at least sonic):

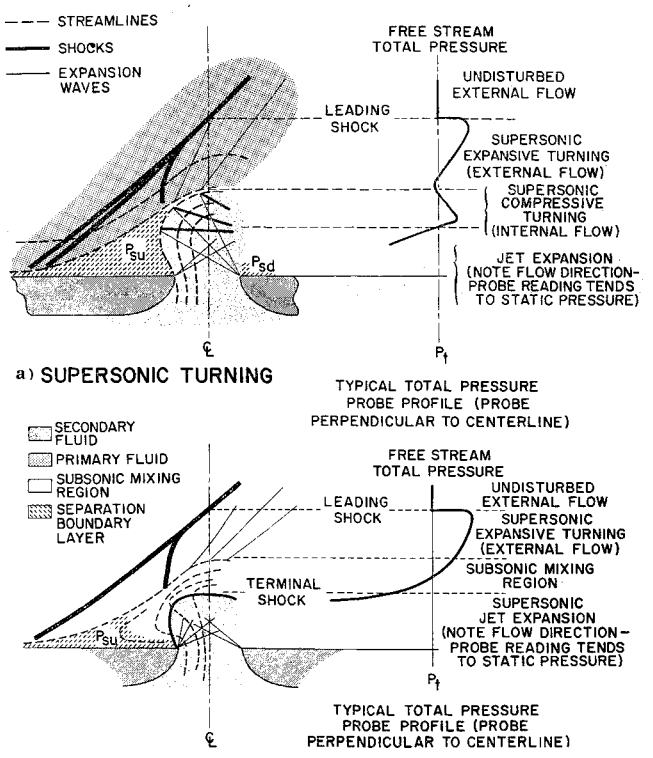

Fig. 10 Schematic description of two possible types of flow in the impingment zone immediately over the injection orifice in the plane of symmetry.

Table 3 Ratio of the jet exit pressure to the undisturbed ambient pressure

	Test	P_j/P_i
Supersonic turning:	C1	6.9
	C2	5.1
Terminal shock:	A1 and B1	5.3
	A2 and B2	3.9
	A3 and B3	2.0
	C3	2.5

1) If $P_j/P_{sv} < 1$, the streamtube must recover through a normal shock preceded by a Prandtl-Meyer expansion at the corner to a Mach number such that the stagnation pressure behind the shock equals P_{su} in analogy with the mechanism evoked earlier in connection with the termination of the jet flow along the centerline.

2) If $P_j/P_{sv} > 1$, the jet-edge streamtube issues supersonically after a centered expansion to a static pressure equal P_{su}.

In the first instance, the occurrence of a shock segment at the upstream nozzle edge, which is well founded, strongly suggests that the whole upstream quadrant of the jet is terminated by a strong shock cap followed by a subsonic flow turning layer, as sketched on Fig. 10b. The terminal shock is located in each individual streamtube so as to match the pressure-deflection characteristic of the external flow around the "equivalent body" of the cap. The profile of pressures that would be recorded by a tube parallel to the nozzle axis can be deduced by inspection of the assumed flow structure. It is shown next to the sketch, and should be compared with the first group of profiles shown on Fig. 9.

In the second instance, the jet can turn downstream supersonically through a system of radiated and reflected waves as sketched on Fig. 10a. The mechanism is the same as that which establishes the shape of the plume of an axisymmetric free jet.[9] The flow is characterized by the fact that the secondary and the main streams are separated by a slipline (not a shock) and by the formation of a "barrel shock" (terminology of jet plume analysis) resulting from the coalescence of the compressive turning waves radiated into the jet field. As before, a typical pressure profile derived from inspection of the proposed flow structure is given next to the sketch. It should be compared with the second group of tests on Fig. 9 (see also Ref. 10).

An inspection of the sketches of Fig. 10 serve better than words to show that the proposed structure of the flow is self-consistent and compatible with all the data. Nonetheless, it is only an interpretation of incomplete observations, and it is quoted here because the striking difference in the measured profiles could not be left without some consideration. A partial quantitative argument for the hypothesis is provided by a study of the conditions under which the changeover from one to the other type of profile was observed. The following ratios of jet exit static pressure to local (undisturbed) nozzle pressure characterized the tests as shown in Table 3. The changeover occurred at about $P_{su}/P_i = 5.2$. This is well within the range of pressure ratios near recompression for upstream-facing steps in turbulent boundary layers, which is $4 < P_{su}/P_i < 6$.

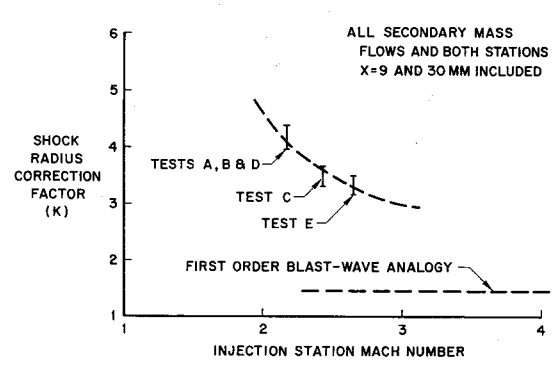

Fig. 11 Correlation of the radii of the leading shock (see Table 2).

Shape and Strength of the Leading Shock

The shape and the strength of the leading shock are essential input quantities in several of the analytical models of secondary injection and therefore deserve separate consideration. We have available two precise comparative experiments in which the shock strength and position were accurately defined. These are the traverses at stations 9 and 30 mm downstream of injection (one of which is shown in Fig. 8). Table 2 summarizes the measured shock radii in the meridional plane (origin at the wall) and also calculations that will be described later.

Throughout this report, shock radii are measured from the wall of the nozzle and not from a line parallel to the axis. The divergence angle of the present nozzle is too small to distinguish clearly between one and the other definition.

The shock shape in cross-sectional planes is not quite self-similar: Fig. 2 (nearer to injection) shows it to be slightly elliptical with the major axis in the meridional plane, but on Fig. 3 (further downstream from injection) it has become circular about an origin at the wall. The recompression shock, which begins to be clearly defined on Fig. 3 and becomes clearer still at stations further downstream (not shown in this paper), is always approximately circular with an origin at the wall.

The most promising analytical model for the radius of the leading shock is based on an analogy with blast-wave theory,[8] and gives, for the shock radius, the relation

$$\frac{R_s}{R_{so}} = \left(\frac{2}{J_0^{1/2}}\right)^{1/2} M_\infty \left(\frac{X_s}{R_{so}}\right)^{1/2} \tag{1}$$

X_s is the shock streamwise coordinate measured from its origin and M_∞ (as well as other quantities with the subscript ∞) is an "equivalent" freestream, uniform flow Mach number.

The reference radius R_{so} was computed and listed in Table 2 for the present tests with the following interpretation of the "blast" energy per unit length:

$$R_{so} = \frac{1}{(2\pi)^{1/2}} \left(\frac{E}{P_\infty}\right)^{1/2} \tag{2}$$

$$E = \frac{m_j h_{j0}}{V_\infty} = \frac{m_j c_p T_{j0}}{V_\infty} \tag{3}$$

$$P_\infty V_\infty = m_\infty \frac{RT_\infty}{A_\infty} \tag{4}$$

$$R_{so} = \frac{1}{(2\pi)^{1/2}} \left\{\left(\frac{T_{j0}}{T_0}\right)^{1/2} \frac{\gamma}{\gamma - 1} \left[\frac{T_0}{T_\infty} \frac{A_\infty}{A_\infty{}^*}\right] \frac{P_{j0}}{P_0}\right\}^{1/2} (A_j{}^*)^{1/2} \tag{5}$$

$$= \frac{1}{(2\pi)^{1/2}} \left\{\frac{T_{j0}}{T_0{}^{1/2} P_0} \frac{\gamma}{\gamma - 1} \left[\frac{T_0}{T_\infty} \frac{A_\infty}{A_\infty{}^*}\right]\right\}^{1/2} (m_j)^{1/2}$$

In order to relate Eq. (1) to experiment, we rewrite it in the following form:

$$\frac{R_s}{R_{so}} = K M_\infty{}^{-1/2} \left(\frac{x - x^*}{R_{so}}\right)^{1/2} \tag{6}$$

where x^* is the distance between the physical coordinate origin (the center of the injection port) and the origin of the blast-wave shock, and K is a numerical constant. The two experimental points at the 9- and 30-mm stations for each test allow us to determine both of these. The first result is $x^* \simeq$

0. It varies from test to test within limits not exceeding the diameter of the injection port, which is negligible in comparison with x at the station 30-mm downstream.

Values of K using $x^* = 0$ and the shock coordinates are tabulated in Table 2. For the analogy to be completely valid, K should remain constant for all test settings. It is found that it does so for all the data pertaining to a given injection-station Mach number, but Mach number effects are not adequately correlated.

The blast-wave analogy is not formally valid at Mach numbers as low as the injection Mach numbers used in this research (and in many TVC applications). It is, therefore, not surprising to find a Mach number effect in the correlation. As the injection Mach number increases and the "blast-wave" analogy becomes more accurate, the value of K should tend toward

$$K_{\text{lim}} = (2/J_0^{1/2})^{1/2}$$
$$= 1.46 \qquad \text{for} \qquad \gamma = 1.4$$

In this sense, the trend exhibited by K based on the present results is reasonable. This is plotted on Fig. 11. Until more evidence becomes available, a correlation curve passing through the measured points and bending asymptotically to K_{lim} can be suggested for use in connection with Eq. (8) in computations of the shock radius.

The strength of the leading shock should also be correlated by the blast-wave similarity parameter, that is,

$$P_s/P_\infty M_\infty \sim (R_{so}/x) \tag{7}$$

In Eq. (7), P_s and P_∞ are static pressures immediately after and before the shock, respectively. The static pressure ratio can be computed from the impact pressure ratio and the Mach number immediately ahead of the shock by use of oblique shock relations.

The data are plotted on Fig. 12. The Mach number appearing in Eq. (7) [as well as in Eqs. (5) and (6), which served to calculate R_{so}] was identified with the Mach-number at the injection station. The data at all stations and all injection Mach numbers are well correlated.

In general, the present measurements confirm that the similarity parameters of the blast-wave analogy are remarkably successful in correlating experimental data. However, this seems to be where the "analogy" ends; for instance, the linear behavior of Eq. (7) prescribed by the theory is not reproduced (see Fig. 12). This is not surprising in view of the obvious discords between the present situation and the blast-wave theory, which formally supposes a self-similar, axisymmetric, small-disturbance hypersonic flow. It would therefore seem proper to de-emphasize this aspect of the analysis and to rederive the correlation parameters in question from a set of fundamental assumptions. This can be done by stating that the only significant physical characteristic of the disturbance is the energy (or momentum) added to the flow, and that the freestream is adequately described by the pressure (P_∞) and the velocity (V_∞) at the injection station. It follows from dimensional analysis that the only possible length-scale for the problem is R_{so} as given by Eq. (2).

This viewpoint may prove more useful in seeking improvements in the correlation than further work on refining the "analogy" with similarity solutions for a one-dimensional explosion.

Conclusions

Aside from contributing new data on the pressure field, this investigation clarifies the nature of the interaction between the secondary jet and the main flow in regard to the following points.

1) The disturbed flow downstream of the injection port is shown to contain three fairly distinct regions, which are (see Fig. 6): an "inner core" of secondary fluid, a spiral-flow mixing zone flanking the inner core and an outer shell of disturbed primary flow contained by the main shock.

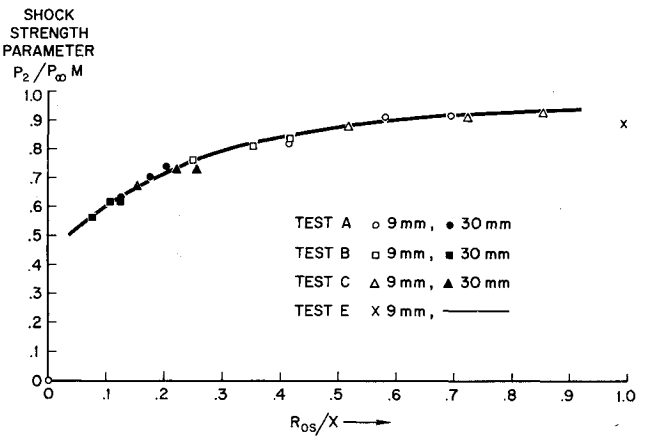

Fig. 12 Correlation of shock strengths.

2) The "penetration height" of the secondary jet, which sets the extent normal of the wall of the inner core and the spiral zone, is determined by the geometry of the shock structure occurring in the secondary jet. It can be of two types, depending on the secondary stagnation pressure: The "terminal shock" interaction and the "supersonic-turning" interaction. This phenomenon means, for example, that the penetration height of the secondary jet is not a simple function of jet momentum.

3) The properties of the leading shock, and thus of the over-all extent of the disturbance, can be correlated well in terms of a dimensionless scale obtained by stating that the only physical quantities describing the interaction are the disturbance energy (or momentum) and the freestream pressure and velocity. This leads to the same correlation parameter as that derived from assuming an equivalence with the hypersonic small-disturbance similarity solution to an explosion (blast-wave analogy). The dimensional-analysis argument is preferred over the second because conceptually and quantitatively the "blast-wave analogy" is not strictly valid in the present situation.

References

[1] Newton, J. F., Jr. and Spaid, F. W., "Interaction of secondary injectants and rocket exhaust for thrust vector control," ARS J. **32**, 1204–1211 (1961).

[2] Cubbison, R. W., Anderson, B. H., and Ward, J. J., "Surface pressure distributions with a sonic jet normal to adjacent flat surfaces at Mach 2.92 to 6.4," NASA TN D-580 (February 1961).

[3] Dupuichs, G., "Mecanisme de la deviation d'un ecoulment supersonique par un jet transversal," Tech. Sci. Aeronaut. Spaciale **2**, 130–142 (1962).

[4] Amick, J. L. and Hays, P. B., "Interaction effects of side jets issuing from flat plates and cylinders aligned with a supersonic stream," Wright Air Development Div. TR 60-329 (June 1960).

[5] Walker, R. E., Stone, A. R., and Shandor, M., "Secondary gas injection in a conical rocket nozzle," AIAA J. **1**, 334–338 1963).

[6] Ferran, C., "Interference between a jet issuing laterally from a body and the enveloping supersonic stream," Johns Hopkins Univ., Applied Physics Lab., Bumblebee Rept. 286 (April 1959).

[7] Wu, J.-M., Chapkis, R. L., and Mager, A., "An approximate analysis of thrust vector control by fluid injection," ARS J. **31**, 1677–1685 (1961).

[8] Broadwell, J. E., "An analysis of the fluid mechanics of secondary injection for thrust vector control," Space Technology Labs. Rept. 6120-7744-MU-000 (March 1962).

[9] Adamson, T. C. and Nicholls, J. A., "On the structure of jets from highly underexpanded nozzles into still air," J. Aeronaut. Sci. **26**, 16–24 (1959).

[10] Heyser, A. and Mauer, F., "Experimentelle Untersuchunden an Festen Spoilern and Strahlspoilern dei Machschen Zehlen von 0.6 bis 2.8," Z. Flugwiss. **10**, Heft 4/5, 110–130 (1962).

[11] Charwat, A. F. and Allegre, J., "Experimental study of the aerodynamic interaction generated by secondary gaseous injection into a supersonic nozzle," United Technology Center TM-33-63-U7 (October 1963).

[12] Lord, W. T., "On axi-symmetrical gas jets with application to rocket jet flow fields at high altitudes," British Aeronautical Research Council R & M 3235 (1961).

NOVEMBER 1964 AIAA JOURNAL VOL. 2, NO. 11

Fuel Sloshing in a Spherical Tank Filled to an Arbitrary Depth

WEN-HWA CHU*
Southwest Research Institute, San Antonio, Texas

The kernel function for liquid sloshing in a spherical tank filled to an arbitrary depth is shown to be related to Green's function of the second kind and is constructed successfully by numerical means. Natural frequencies are then computed as eigenvalues of a matrix. Eigenfunctions are obtained, at a finite number of points, as the eigenvectors that are sufficient for approximate evaluation of the force acting on the container. Simple formulas of force and moment are given for both pitching and translational oscillation under a fixed gravitational field. Finally, comparisons of both predicted natural frequencies and force response with the experimental results for a quarter-full tank are given.

Nomenclature

a = radius of the spherical tank
A_F = area of undisturbed free surface
A_R = area of wetted surface of sphere
b = maximum value of ρ, radius of free surface
d = tank diameter, $2a$
C_{ij} = g_{ij}
$D(q)$ = $[E(q) - K(q)]/q^2$
$D(\beta, k')$ = $[E(\beta, k') - k' \sin\beta]$
$DKEF$ = a function in the computer program (cf. Appendix C)
F = undisturbed free surface
F_s = horizontal force acting on the tank due to fuel sloshing
F_{ij} = $(\rho_i\rho_j)^{1/2}F_0(\rho_j, \rho_i) = F_{ji}^{(0)}$ (note the order of ρ_i, ρ_j in F_{ij})
$F_0(\rho, \rho')$ = integrated kernel function related to $\partial G_0/\partial n$
g = effective gravitational acceleration
g_{ij} = $(\rho_i\rho_j)^{1/2}h_1(\rho_i, \rho_j)$
$G(P, Q)$ = Green's function of the second kind for the spherical bowl
$G_0(P, Q)$ = Green's function of the second kind for a sphere
$h(P, Q)$ = additional part of Green's function for spherical tank other than half-full
$h_1(\rho, \rho')$ = integrated kernel function related to $h(P, Q)$
$H(\rho, \rho')$ = integrated kernel function related to $G(P, Q)$
$H_0(\rho, \rho')$ = integrated kernel function related to $G_0(P, Q)$
H_{ij} = $(\rho_i\rho_j)^{1/2}H(\rho_i, \rho_j)$
$H_{ij}^{(0)}$ = $(\rho_i\rho_j)^{1/2}H_0(\rho_i, \rho_j)$
I = point of integration, except $[I]$ being the unit matrix
$K(q)$, $E(q)$ = complete elliptic integrals of first and second kind, respectively
M_L = total mass of liquid (fuel)
n = outer normal
$NEFF$ = a function in the computer program (cf. Appendix C)
$P(Q)$ = $[K(q) - (\pi/2)]$ (cf. Appendix C)
$\bar{P}(r, \psi)$ = a ring corresponding to $P(r, \psi, \theta)$
q_1 = $2(\rho\rho')^{1/2}/(\rho + \rho')$
q_2 = $2a(\rho\rho')^{1/2}/[(\rho\rho' - b^2)^2 + z_F^2(\rho - \rho')^2 + 4\rho\rho'a^2]^{1/2}$
$\bar{Q}, \bar{I}$ = analogous to P but related to Q and I, respectively
r, ψ, θ = spherical coordinates
R = the wetted spherical surface before sloshing unless defined by (A2)
$R'(P, P')$ = $[r'^2 + (a^4/r^2) - 2(r'/r)a^2\cos\gamma]^{1/2}$
R_{PQ} = distance between the points P and Q
dS = element of surface
$d\bar{S}$ = $dS/d\theta \to \rho d\rho$ on F
U = horizontal displacement of container in the x direction
x = $r\cos\theta$
z_F = vertical distance of free surface from center of sphere; positive upward
α_n = defined by Eq. (11b) $\int_F \phi_n^2(I)dS_I$
β_n = defined by Eq. (11a)
$\cos\gamma$ = angle between the vectors **OP** and **OP'**
λ_1, λ_2 = $(1/\rho\rho')\{-z_F^2 \pm [z_F^4 + z_F^2(\rho^2 + \rho'^2) + \rho^2\rho'^2]^{1/2}\}$, respectively
$\Lambda_0(\psi, q)$ = Heuman's lambda function (Ref. 9)
$\tilde{\lambda}_n$ = ω_n^2/g
$\Pi(\alpha^2, q)$ = complete elliptic integrals of the third kind (Ref. 9)
ρ = radial distance from a point on the free surface to the center of the free surface
ρ', ρ_j = ρ of integration variable
ρ_L = density of liquid (fuel)
ϕ_v = velocity potential, $\nabla\phi_k = \mathbf{q}$, $\mathbf{q}$ being the velocity vector

Received June 6, 1963; revision received July 27, 1964. The material in this paper is condensed from Ref. 1 and from Part I, Sec. 3 of Ref. 2. The research was originally supported by the Army Ballistic Missile Agency under Contract DA-23-072-ORD-1251 and was completed under an internal research program of the Southwest Research Institute. The author would like to express his deep appreciation to Robert Gonzales for his industrious effort in programing as well as checking most parts of the present theory and to Thomas Jackson for his consultation and assistance in part of the programing. Also, the author would like to express his appreciation to Thein Wah and William Squire for their informative discussions. Finally, the author would like to thank H. N. Abramson for his discussions and his continued support, without which the present research could not have been completed.

* Senior Research Engineer. Member AIAA.